Nov-2007

Muon Capture on the Deuteron

The MuSun Experiment

Preliminary, not for distribution

MuSun Collaboration

Abstract: We propose to measure the rate for muon capture on the deuteron with 1% precision. At such high precision, this reaction will provide a benchmark result on weak processes in the two-nucleon system, far more precise than all experimental information at present and in the foreseeable future. Moreover, it can impact fundamental reactions of astrophysical interest, like solar pp fusion and the $\nu + d$ reactions observed by the Sudbury Neutrino Observatory. Recent effective field theory calculations have demonstrated, that, up to next-to-next-to-leading-order, all these reactions are related by one axial two-body current term, parameterized by a single low-energy constant. Muon capture on deuterium can determine this constant precisely and thus comes closest to calibrating these basic, but extremely slow electroweak processes under terrestrial conditions.

Experimental method, to be completed. This 10 fold improvement in precision compared to earlier experiments is feasible due to the advanced techniques developed for the MuCap experiment [3]. As in the case of the MuCap experiment, utmost care is required to eliminate uncertainties due to muon atomic physics effects. Thus, while the general experimental strategy is similar to MuCap, a new cryogenic TPC operating at gas densities of up to 10% of LH_2 will be developed to ascertain optimal conditions for an unambiguous interpretation of the experiment.

Contents

1 Beam Requirements

* beam line , area, special facilities (Separators, SC magnets, spectrometers)
* beam properties (type of particle, intensity, momentum....)
* duration of the experiment (time for setting up, tests, production runs)
* any special conditions
* beam time request for the first beam period after approval

2 Safety Sheet

The third page should consist of the declaration sheet for hazardous samples/equipment (PDF, Word) . This does not replace a detailed description of safety questions in the full text of the proposal.

Safety Procedure for R-Experiments

The purpose of this document is to guide applicants for R-Experiments (experiments at the 590 MeV Ring Cyclotron) through the different safety regulations and procedures applicable at PSI concerning hazardous equipment and sample material.

General

If you intend to work with hazardous equipment and material, the first persons to be contacted are the Safety Officers of your home institution. They must inform you about all potential risks involved. They will also inform you about the regulations applicable in your country.

The Responsibility for Hazardous Equipment and Sample Material at PSI lies with the Experiment Spokespersons. In case of a test experiment the coordinator of these tests is responsable for safety. The PSI safety procedures listed below are obligatory for them.

The Safety Officers of PSI are available to help you fulfilling the necessary regulations applicable to PSI. You must contact them well in advance.

Safety of your equipment.

In designing your experiment or in case you change your approved experimental set-up, you should proceed as follows:

1. Contact the Coordinator for R-Experiments to discuss the instrument's design or planned modifications. 2. Use the Declaration Sheet for Hazardous Sample/Target Material and Experimental Equipment (PDF, Word) of the Safety Committee PSI West to characterize the hazards of your equipment. Add the Declaration sheet to your proposal. You are in addition requested to describe the safety risks of your experiment in the text of your proposal. 3. When the design of the equipment is finalized, contact the appropriate members of the Safety Committee. The Safety Officers will discuss with you the necessary safety precautions and authorisations for your equipment. 4. Before installing new or modified equipment at PSI for the first time, contact the Safety Committee again to allow inspection of your equipment.

Hazardous sample material.

When you intend to investigate hazardous sample material (radioactive, toxic, flammable, etc.) on your experiment, proceed as follows:

1. Use the Declaration Sheet for Hazardous Sample/Target Material and Experimental Equipment (PDF, Word) of the Safety Committee PSI West to characterize the hazards of your sample. 2. Contact the appropriate members of the Safety Committee well in advance. The Safety Officers will discuss with you the necessary safety precautions, authorisations and handling procedures.

year	ref	method	L_1A	σ_1	σ_2	comment
2 body						
2002	BCV [9]	$\bar{\nu} + d$	3.6	4.6	5.5	best exp ± 8.1, correlations, χ^2
2003	CHR [11]	ES, CC, NC SNO	4.0	6.3	6.7	error $\sim 5fm^3$ in future
3 body						
1998	Schiavilla [20]	tritium decay	4.2	0.1	3.7	3B system in SNPA and hybrid EFT only
2006	Marcucci [19]	μ^3He				
other						
2002	BBG [8]	helisoseismology 4.8	7	5.9	6.7	other solar model uncertainties

Table 1: Table of L_{1A} compilation. Uncertainty σ_1 for 2B processes assumes that $\sim 3\%$ uncertainty of N^{3}LO ($\not\pi$EFT) similar for all processes. σ_2 includes this uncertainty.

3 Physics Motivation

The MuSun experiment aims to measure the rate Λ_D for the semileptonic weak process

$$\mu^- + d \rightarrow \nu_\mu + n + n \tag{1}$$

with a precision of 1-precent or better. The index d denotes the capture rate from the doublet hyperfine state of the muon deuterium atom in its 1S ground state. The experiment would exceed the precision of previous experiment by an order of magnitude. In this section the motivation for the experiment is presented in a more general context. The physics and status of reaction 1 is discussed in section 4.

3.1 Calibration of Fundamental Astrophysics Reactions

What is the big picture?

How different/cleaner than hybrid EFT and tritium?

Expected precision in L1A? L1A table.

What impact on neutrino physics?

3.2 Benchmark Electroweak Reaction on the Deuteron

Big picture progress/effort in EFT with nucleons.

Axial 2N reactions not directly constraint, information scarce (compare with NPDG).

Theoretical program connected with MuSun Experiment.

3.3 Additional Impact

Polarization observables in muon capture. Form factors.

Muon capture and muon-catalyzed fusion probe other elusive reactions.

Technology. Collaboration with FermiLab, other applications of hydrogen TPC.

4 Muon Capture on the Deuteron

4.1 Theory

The muon capture reaction 1 results from the same hadronic current as muon capture on the free proton, which is currently measured with high precision by the MuCap collaboration [3]. Its rate Λ_D from the doublet state of the $d\mu$ atoms shows a similar sensitivity to g_P as Λ_S. There are additional interesting features. The final 3-body state covers a broad range of momentum transfer to the 2-N system (see Fig.1). In adequate non-relativistic kinematics the total energy $Q = 102.1\ MeV$ in the final state is the sum of the neutron CMS energy, two neutron relative energy E_{nn}, and the neutrino momentum p_ν.

$$Q = \frac{p_\nu^2}{4M_n} + E_{nn} + p_\nu \tag{2}$$

Thus the kinematics can be parametrized either by E_{nn} or equivalently by p_ν. The properties of the 2-N system enter, in particular the deuteron wave function in the initial and the neutron scattering length a_{nn} in the final state. Furthermore, two-body currents contribute, making process (1) uniquely suited to study the axial 2-body currents in the 2-N system.

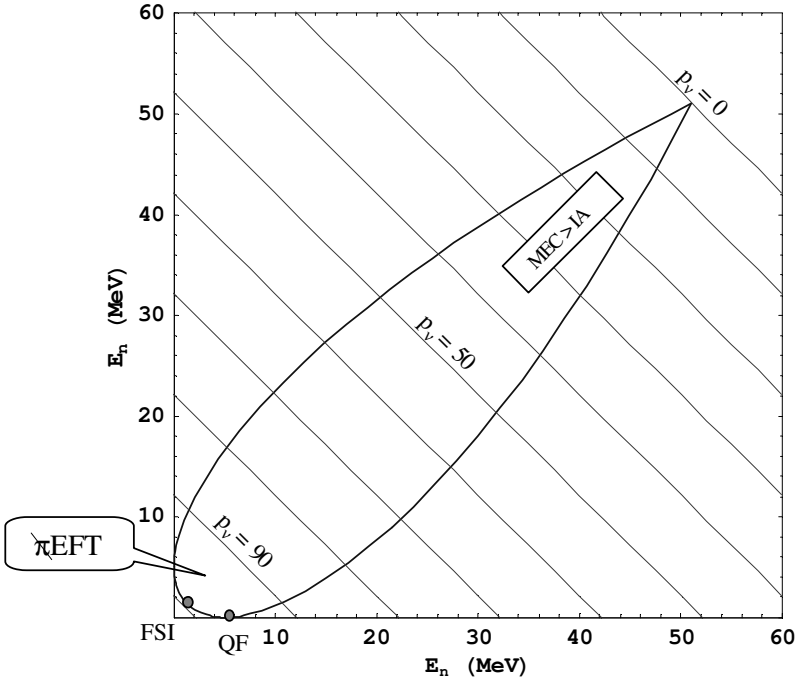

Figure 1: μd capture Dalitz plot as function of neutron energy. Diagonal lines indicate constant neutrino momentum p_ν (MeV/c). Interesting kinematic regions include: final state interaction ; quasifree ; $p_\nu \geq 90 MeV/c$, where pionless EFT applies; small p_ν, where MECs dominate over impulse approximation.

Muon capture on the deuteron is successfully described by two frameworks, the standard nuclear physics approach (SNPA) and by effective field theory (EFT) calculations. The most sophisticated SNPA calculation were performed around 1990 [21, 1, 14]. Thereafter the concept of effective field theories in the form of chiral perturbation theory (χPT) was expanded to the 2N system. The latest calculation were performed in hybrid EFT [2] and most recently in pion-less EFT [12] ($\not\pi$EFT). Fig. 2 summarizes the theoretical and experimental results.

Current calculations agree that the one body (1B) operators are very well defined. The challenge lies in the short range part of the axial two body current (2B). In the meson exchange (MEC) picture it is dominated by the πNN^* isobar current, which is not constraint by general symmetry principles. The systematic expansion of χPT demonstrated that exactly the same combinations of low energy constants (LECs) appear in the two body reactions $p+p$ fusion, $\nu+d$ scattering and $\mu+d$ capture. The hybrid EFT used tritium beta decay to constrain the unknown LEC. The $\not\pi$EF treats this LEC called L_{1A} as an unknown parameter and parametrizes the capture rate as

$$\Lambda_D = a + b\ L_{1A} \tag{3}$$

where a and b depend on the E_{nn} Dalitz plot cut. E.g. for $E_{nn} = 5\ MeV$, a=$239.2 s^{-1}$and b=$3.3 s^{-1} fm^{-3}$. Both calculations agree if $L_{1A} = 5.6\ fm^3$ is used [12] . The hybrid EFT calculation estimates an uncertainty 1%, resulting from small dependence on cutoff parameter, tritium beta decay rate, higher MEC contributions and a conservative estimate of the $L \geq 1$ partial waves. It also notes that radiative corrections still need to be calculated. The $\not\pi$EF paper concludes that its uncertainty of 2-3% is dominated by N^3LO contribution, not yet calculated.

Mention differential oservables. In particular spin correlation (asymmetry) potentially accessible ofr the first time in muon capture on muonic hydrogen isotopes.

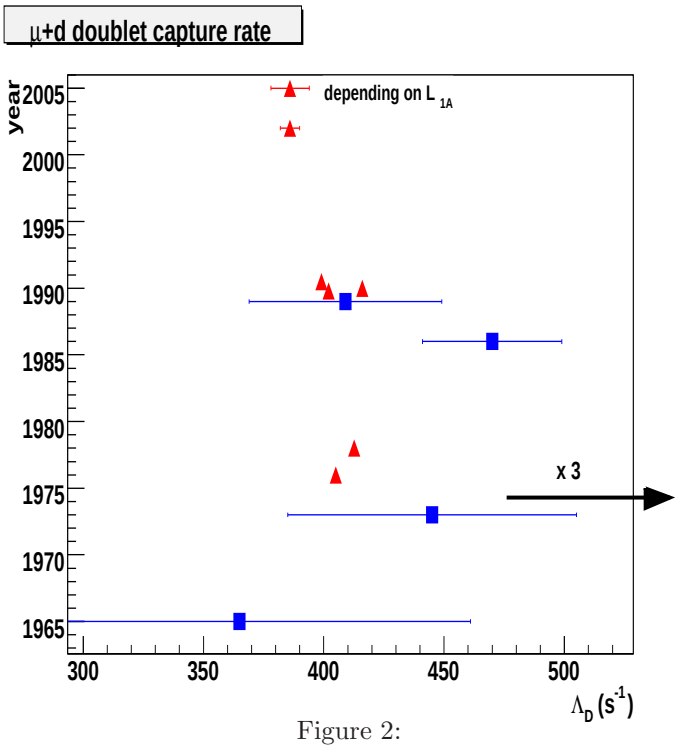

Figure 2:

4.2 Experiment

The early counter experiments were based on the observation of capture neutrons. While a precise measurement of the absolute neutron emission rate is difficult even for 5.2 MeV neutrons resulting from μp capture, it is even harder for the continuous spectrum of neutrons emitted in μd capture which is peaked at 1.5 MeV. Moreover, numerous 2.45 MeV neutrons are produced by muon catalyzed dd fusion, representing a significant background. The interpretation of the experiments requires an accurate knowledge of dμ hyperfine population at the moment of capture, because the V-A structure of weak interactions suppresses capture from the quartet relative to the doublet state. The first generation experiments[22, 6] tried to reduce the background from dd fusion, by using hydrogen targets with small deuterium concentration. Because of the fast pμ to dμ transfer rate, such a target acts as an effective hydrogen target. The price to pay for such an approach is that at high densities capture occurs from a molecular state and the background from μ^3He build-up is significant. For lower densities, on the other hand, the dμ hyperfine population was essentially unknown at that time and had to be conjectured as being pure doublet.

year	ϕ(%)	c_D(%)	T (K)	detection	statistics	Λ_d(s^{-1})	comment
1965	100	0.32	20	neutron	615	365±96	dominant μ^3He
1973	0.76	5	300	neutron	6295	445±60	corrected to $\approx$ 1335 ± 180 *)
1986	100	100	20	electron	5 10^8	470±29	
1989	4	100	45	neutron	$\approx$ 2000	409±40	

Table 2: Counter experiment on $\mu + d$ capture. Density ϕ normalized to LH_2 density. Experiments performed in D+H mixtures, with c_D given in column 3. *) Original Result has to be scaled up, because experiment corresponds to mostly statistical, not doublet dμ hyperfine population.

The situation changed with the discovery [16] of a strong dependent temperature hyperfine effect in resonant ddμ formation, which made the dμ hyperfine population directly experimentally accessible. This and subsequent experimental and theoretical work proved that the conditions in experiment [6] were statistical, so the observed experimental rates should be scaled by a factor of 3 to be converted into Λ_d, according to the statistical weight of the doublet state. The resulting contradictory situation stimulated a new generation of experiments based on pure deuterium targets.

One innovation [5] was the detection of electrons with a liquid target at Saclay, which avoided neutron detection and background from dd fusion. Lifetimes of both μ^- and μ^+ were measured with an accuracy of a few times 10^{-5}. The muon lifetime measurement started 1 μs after the beam burst, after muons stopped in wall materials were already captured. The final rate included corrections for protium ($c_P = 0.13\% - 0.18\%$), μ^3He capture $\delta\Lambda = (60 \pm 16)\ s^{-1}$ as well as instrumental effects.

The Vienna PSI experiment [10] on the other hand used neutron detection, but reduced the gas density and temperature to suppress fusion neutrons and performed supplemental analyses with high neutron threshold above the 2.5 MeV fusion neutrons. In the low density target the stopping fraction of muons in D_2 was $(75.7 \pm 1.7)\%$. The physics background, consisting of carbon stops, diffusion, photo neutrons and fusion neutrons, exceeded the physics signal by a factor of 1.4 and uncertainties in its subtraction dominated the error of the final result.

The current overall experimental situation on Λ_D (see Fig.2) is quite unsatisfactory. The best two measurements were performed almost two decades ago. They have uncertainties of 10-15% and are only marginally consistent, with the more accurate experiment deviating from theory by 2.4 σ.

4.3 Status of Basic Muon Capture Reactions

Discuss mu+p, mu+d and mu+3He, including the recent rad corr update [13]. Can we trust the 0.5% precision of calculation [18].

4.4 L_{1A} extraction

The current theoretical uncertainty for Λ_D ranges from 1-3%. Assuming an experimental determination of Λ_D with 1% precision L_{1A} would be determined as

$$\delta L_{1A} \sim \frac{a}{b}\sqrt{\frac{\delta\Lambda_D^{th\,2}}{\Lambda_D^{th}} + \frac{\delta\Lambda_D^{exp\,2}}{\Lambda_D^{exp}}} \tag{4}$$

which gives

$\frac{\delta\Lambda_D^{th}}{\Lambda_D^{th}}(\%)$	$\delta L_{1A}(fm^{-3})$
0	0.71
1	1.0
2	1.2
3	1.4

Given this impressive precision claimed we critically discuss uncertainties due to additional physics input. The sensitivity to g_P is $\frac{\delta\Lambda_D}{\Lambda_D}/\frac{\delta g_P}{g_P} = 0.2$. Thus final MuCap result for g_P at the 1% level, is a prerequisite for determining L_{1A} from muon capture. The g_P uncertainty will contribute $\frac{\delta\Lambda}{\Lambda} = xx\%$. NEEDs discussion on uncertainty reduction if capture rates are compared, theory also. The dependency on the neutron scattering length a_{nn} would only lead to $\frac{\delta\Lambda}{\Lambda} = 0.9\%$, if the currently accepted value of $a_{nn} = -18.6 \pm 0.4\ fm$ is being used. This value is derived exclusively from the $\pi d \to n + n + \nu$ reaction and does not take the deviating results for n+d break-up into account [17, 15].

5 Experimental Strategy

Advanced state. Needs setup figure, improved rate figure, kinetic fit. Plus checking by Claude and PNPI.

5.1 Overview

In order to achieve the goal of this experiment two main conditions have to be met.

- The measurement must be performed at conditions, such that the experimental result leads to an unambiguous extraction of Λ_d, independent from muonic atomic physics uncertainties.
- The measurement must achieve an overall precision of 1% of Λ_d ($4\ s^{-1}$), which is an order of magnitude higher than achieved in previous experimental work.

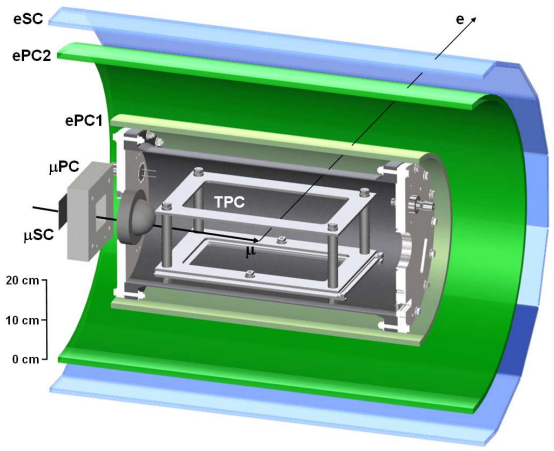

Figure 3: NEEDS UPDATE WITH REAL SET-UP. Simplified cross-sectional diagram of the MuCap detector. The detector components are described in the text.

Muon kinetics and optimal target conditions

The muon induced atomic and molecular processes (*muon kinetics*) are quite different for negative muons in deuterium compared to the muon kinetics in pure protium (relevant for the MuCap experiment). The hyperfine transition rate λ_{qd} of the upper $d\mu(\uparrow\uparrow)$ quartet to the $d\mu(\uparrow\downarrow)$ doublet state is slow. The V-A structure of weak interactions, however, disfavors capture from the doublet state (Λ_q=12 s^{-1}) compared to capture from the doublet state (Λ_d=386 s^{-1}), so that the experimentally observed capture yield is largely proportional to the population of the doublet state. The $d\mu$ system has been intensively studied as the prototype for resonant muon-catalyzed fusion [7]. For a clear interpretation and for the accumulation of sufficient capture statistics, the target conditions should be chosen such that the $d\mu$ doublet state dominates and the population of states can be verified *in-situ* by the observation of muon-catalyzed fusion reactions. Our optimization indicates excellent conditions at $\phi = 5\%$ and T=30 K, which we define as the baseline of the experimental proposal. On the positive side complications from muon capture in the $dd\mu$ molecule are nearly absent, as it is short lived. Moreover, the μd diffusion problem does not exist, as the elastic cross section for μd+d scattering is large. μ^3He formation, isotopic purity and chemical impurities still need careful attention.

Experimental technique for 1% measurement

The 10 fold improved experimental precision is based on the the techniques developed for MuCap. Muons will be stopped in an active gas target consisting of a hydrogen time projection chamber (TPC) operating with chemically and isotopically ultra-pure deuterium. The reconstruction of the muon stopping point in 3 dimensions eliminates the otherwise overwhelming background from muon stops in wall materials. The capture rate is determined using the lifetime technique, that is, from the difference between the measured disappearance rate $\lambda_\mu^- \approx \lambda_\mu^+ + \Lambda_d$ of negative muons in hydrogen and the μ^+ decay rate λ_μ^+, where it is assumed that free μ^- and μ^+ decay with identical rates according to the CPT theorem.

The experimental setup is illustrated in Fig. 3. Incident muons first traverse a plastic scintillator (μSC) and a multiwire proportional chamber (μPC), and then pass through a 0.5-mm-thick hemispherical beryllium window to enter an aluminum pressure vessel filled with ultra-pure, deuterium gas at a pressure of 0.5 MPa and 30 K temperature. In the center of the vessel is the TPC (sensitive volume $10 \times 10 \times 8$ cm^3), which tracks incoming muon trajectories and thus enables the selection of muons that stop in the gas at least 15 mm away from chamber materials. Approximately XX% of the muons passing through the μSC stop within this fiducial volume. The ionization electrons produced by incoming muons drift downwards at velocity XX mm/μs in an applied field of XX kV/cm, towards a pad structured ionization chamber. Signals from the TPC are recorded deadtime free with custom build FADCs. The TPC is surrounded by two cylindrical wire chambers (ePC1, ePC2), each containing anodes and inner/outer cathode strips, and by a hodoscope barrel (eSC) consisting of 16 segments with two layers of 5-mm-thick plastic scintillator. This tracking system detects outgoing decay electrons

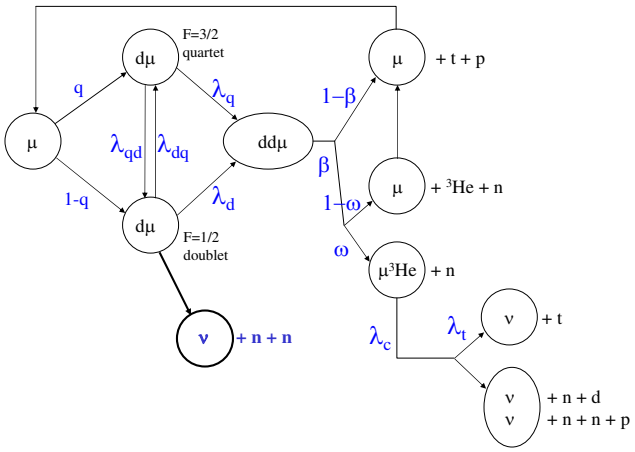

Figure 4: Simplified muon kinetics in pure D_2.

with 3π solid angle acceptance. All data are recorded in a trigger-less, quasi-continuous mode to avoid deadtime distortions to the lifetime spectra.

The electron tracking system, the beam counters, the sophisticated vacuum and purification system and a large part of the electronics and data acquisition can be taken over from the MuCap experiment. The main distinctive features of the MuSun experiment are demanded by physics requirements and include

- High density cryogenic ionization chamber operating as TPC filled with ultra-pure deuterium to define muon stop, identify impurities and to observe muon induced processes.
- Excellent energy resolution of the TPC and full analog readout with FADCs to monitor the charged particles induced by fusion and impurity capture processes.
- Advanced purity monitoring system with new particle detectors and chromatographic methods.
- Neutron detectors to monitor the muon kinetics via capture neutrons and fusion product and separate impurity from fusion signals in the TPC.

5.2 Kinetics

Figure 4 shows a simplified scheme of the muon induced kinetics in pure deuterium[1]. Because of its unique importance for understanding muon-catalyzed fusion, resonant molecule formation and weak interactions, this reaction chain has been scrupulously studied both experimentally and theoretically. The latest experimental results are presented in Ref. [4] which also includes many experimental details relevant for the present proposal. The current knowledge of the relevant parameters is compiled in Fig. 5 and Table 5.2. As is conventional all density dependent kinetic rates have been normalized to LH_2 density N=4.25 $\times$ 10^{22} atoms/cm^3, and the density ϕ is expressed relative to this value.

The vector n(t) for the μd quartet, μd doublet and $\mu^3 He$ state

$$n(t) = \begin{pmatrix} n_q(t) \\ n_d(t) \\ n_3(t) \end{pmatrix} \tag{5}$$

with initial conditions

$$n(t=0) = \begin{pmatrix} q \\ 1-q \\ 0 \end{pmatrix} \tag{6}$$

[1]The simplifications include: The effective ddμ fusion rate has been omitted, since it is nearly instantaneous ($\leq$ 1 ns) at the time scales considered. The hfs dependence of the branching ratio β has been ignored. Small corrections to the kinetics are induced by the finite thermalization time of μd atoms.

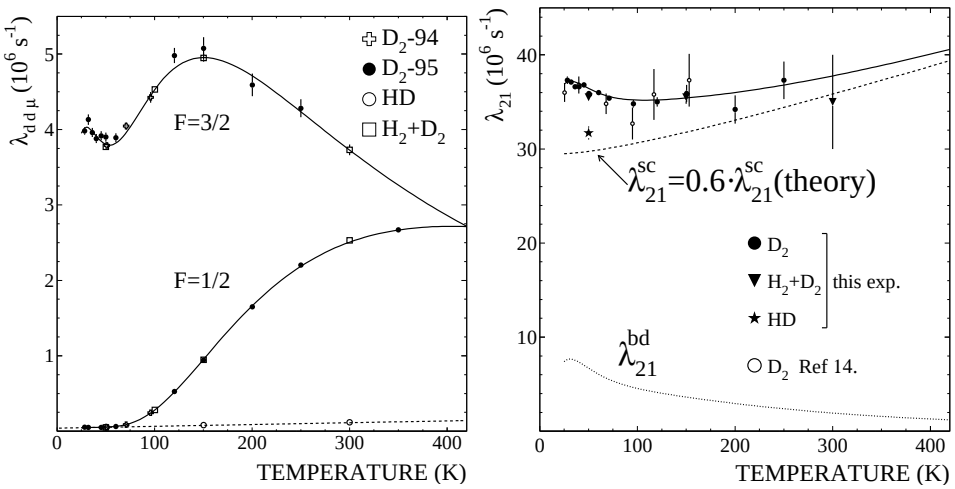

Figure 5: LEAVE OFF HD STUFF, SIMPLIFY Left: $dd\mu$ formation rate λ_q and λ_d; Right: hfs transition rate λ_{qd}.

description	quantity	value	
		300K	30K
initial quartet fraction	q	2/3	
hf transition $q \to d$	$\lambda_{qd}(\mu s^{-1})$	~ 37	37.0(4)
hf transition $q \to d$	$\lambda_{dq}(\mu s^{-1})$	[1)]	
ddμ form. rate from q	$\lambda_q(\mu s^{-1})$	~ 3.75	3.98(5)
ddμ form. rate from d	$\lambda_d(\mu s^{-1})$	2.549(23)	0.053(3)
effective fusion fraction	β	0.590(6)	0.517(15)
sticking probablity	$\overline{\omega}$ [2)]	0.1206(6)	
^{3}He total capture rate	$\Lambda_{He}(s^{-1})$	2216(70)	
^{3}He partial capture rate	$\Lambda_T(s^{-1})$	1496.0(40)	
μd quartet capture rate	$\Lambda_Q(s^{-1})$	~ 8.4	
μd doublet capture rate	$\Lambda_D(s^{-1})$	$\sim$400	

Table 3: CHECK AND UPDATE Kinetic parameters. All values given with error bars are directly determined experimentally, others theoretical. Update with latest values. [1)] $\lambda_{dq} \sim \frac{q}{1-q} e^{-\frac{\Delta}{kT}}$, with the μd hyperfine splitting energy Δ=0.0485 eV and k=8.6174 10^{-5} eV/K (small deviations possible due to back-decay); [2)] it is convenient to define the effective sticking fraction $\omega = \beta\overline{\omega}$.

obeys the following kinetic equations

$$\frac{dn(t)}{dt} = Kn(t) \tag{7}$$

where

$$K = \begin{pmatrix} -\lambda_\mu^+ - \Lambda_q - \phi\lambda_{qd} - \phi\lambda_q(1-q(1-\omega)) & \phi\lambda_{dq} + \phi\lambda_d q(1-\omega) & 0 \\ \phi\lambda_{qd} + \phi\lambda_q(1-q)(1-\omega) & -\lambda_\mu^+ - \Lambda_d - \phi\lambda_{dq} - \phi\lambda_d(1-(1-q)(1-\omega)) & 0 \\ \phi\lambda_q\omega & \phi\lambda_d\omega & -\lambda_\mu^+ - \Lambda_3 \end{pmatrix} \tag{8}$$

The observable time distributions include el(t) for the electrons, fus(t) for the ^3He fusion products, capN(t) for the neutron from $\mu + d$ capture and capT(t) for the tritons from $\mu +^3 He$ capture.

$$el(t) = \quad \frac{dN_e}{dt} = \quad \lambda_\mu^+ \sum_i n_i(t) \tag{9}$$

$$fus(t) = \quad \frac{dN_{^3He}}{dt} = \quad \beta(\phi\lambda_q n_q(t) + \phi\lambda_d n_d(t)) \tag{10}$$

$$capN(t) = \frac{dN_n}{dt} = 2(\Lambda_q n_q(t) + \Lambda_d n_d(t)) \quad (11)$$

$$capT(t) = \frac{dN_T}{dt} = \Lambda_T n_3(t) \quad (12)$$

$$(13)$$

5.3 Optimization of the Target Conditions

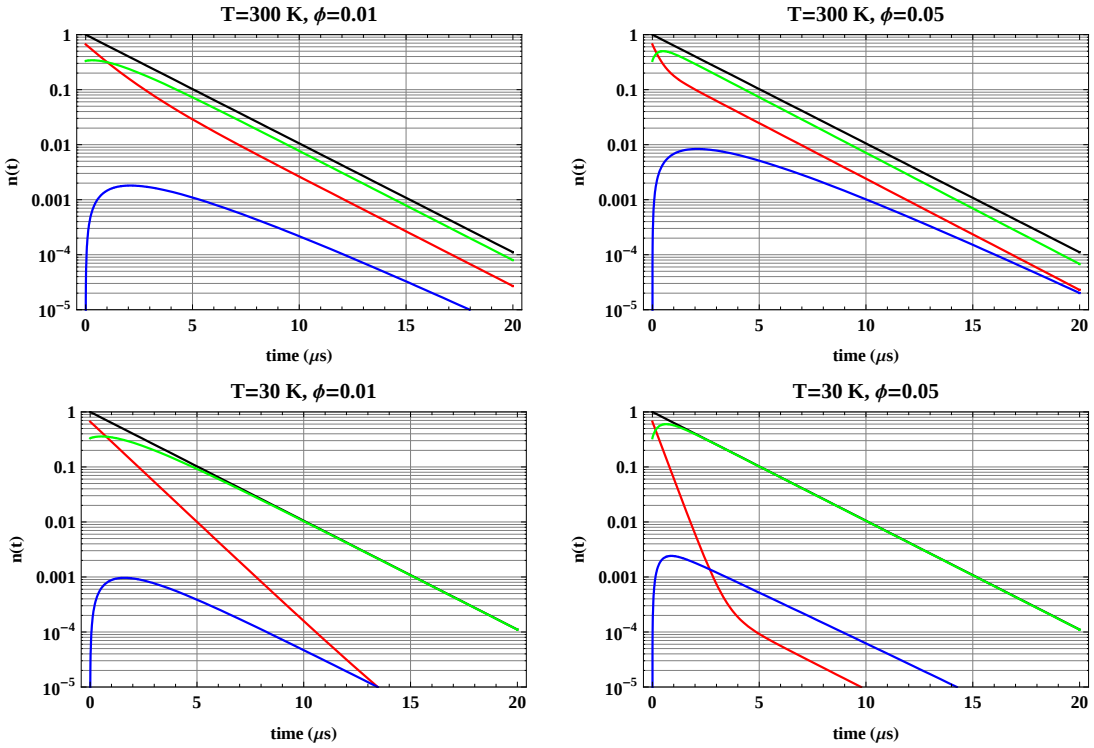

Figure 6: Time distributions of relevant states for different deuterium densities ϕ and temperatures T. μd(black), $d\mu(\uparrow\downarrow)$ (green), $d\mu(\uparrow\uparrow)$ (red), ${}^3He\mu$ (blue).

Fig.6 shows time distribution calculated by numerically solving the full system of linear differential equations Eq.7. The goal of the experiment is the determination of the μd doublet capture rate, thus (i) the doublet population should be maximized (or at least well defined) and (ii) background from μ^3He minimized. To optimize (i), the density should be increased compared to the density ϕ=0.01 of the MuCap experiment. This accelerates the hyperfine transition according to the rate $\phi\lambda_{qd}$. Lower temperatures provide a significant advantage, because the smaller rate λ_d leads to less quartet population (via recycling) and to less μ^3He production (ii). Moreover, at low temperatures the $dd\mu$ formation rates λ_q and λ_d are dramatically different, making it easy to monitor the hyperfine populations via the fusion time distribution fus(t). This fact is clearly demonstrated in Fig.5, where the hyperfine transition rate is determined with high precision at low temperatures whereas the experimental uncertainty increases to 15% at T=300. Finally, T=30 allows for 5 times higher density, while keeping the operating pressure comparable to the MuCap conditions, so that walls and entrance window thickness need not be increased. In summary, based on the physics requirements and practicability of the target design, the conditions ϕ=0.05 and T=30 indicated in the right, lower panel of Fig.6 were chosen as the baseline design of this experiment.

For a systematics study of the error contribution from all relevant quantities we used two methods (first moment method and xxx minimization, which gave consistent results). The baseline conditions were also fitted to Monte Carlo generated data. For the first moment method we define

$$\delta\lambda = \frac{\int_0^\infty n(t)dt}{\int_0^\infty tn(t)dt} - \lambda_\mu^+ \quad (14)$$

where $\delta\lambda$ is an approximation for the difference in disappearance rates $\lambda_\mu^- - \lambda_\mu^+$. We numerically calculate the effect of a parameter α to $\delta\lambda$ as

$$\Delta(\delta\lambda) = \frac{\partial(\delta\lambda)}{\partial\alpha}\alpha\frac{\Delta\alpha}{\alpha} \tag{15}$$

Fig.7 displays the effect of parameter variations on the observable $\delta\lambda$ for $\frac{\Delta\alpha}{\alpha}$=0.1 in α= λ_q, λ_d, λ_{qd}, ω and Λ_{He} compared with the effect of $\frac{\Delta\alpha}{\alpha}$=0.01 in Λ_d (i.e. the measurement goal). The density dependence is easy to understand. At the limit of $\phi << 0.01$ the μd hfs states remain in nearly statistical mixture, therefore the dependence on λ_{qd} is reduced. At the same time, however, the sensitivity to Λ_d decreases as well as the observed capture rate approaches the statistical rate $\approx \frac{\Lambda_d}{3}$. At $\phi >> 0.01$ the hyperfine transition becomes fast, nearly all μ atoms are in the doublet state and, as a consequence, the sensitivity to λ_{qd} is small again. Clearly, sufficient precision is difficult at 300 K, while the uncertainties are below 1 s^{-1} at 30 K and $\phi = 0.05$. At that temperature the relevant parameters are known to better than $\frac{\Delta\alpha}{\alpha}$=0.03, reducing the kinetic uncertainties to a nearly negligible level.

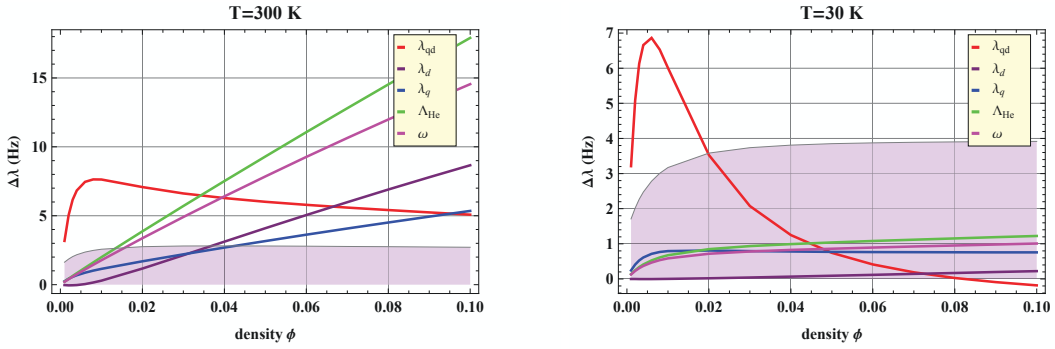

Figure 7: Effect of parameters on the difference $\delta\lambda$ in the observed disappearance rates assuming an uncertainty of 10% in the relevant kinetics parameters. The shaded area indicates the variation of $\delta\lambda$ for a variation of Λ_d by 1%.

Explicit fits of MC data. Include also neutron detectors. I am not sure how the covariances are treated in the first moment and xx minimization method).

6 Experimental Setup

Some figures 8,9,10 are placed here which will be useful for this section.

6.1 Cryogenic TPC

6.2 Cryogenics and Gas system

6.3 Detectors

6.4 Electronics and Data Aquisition

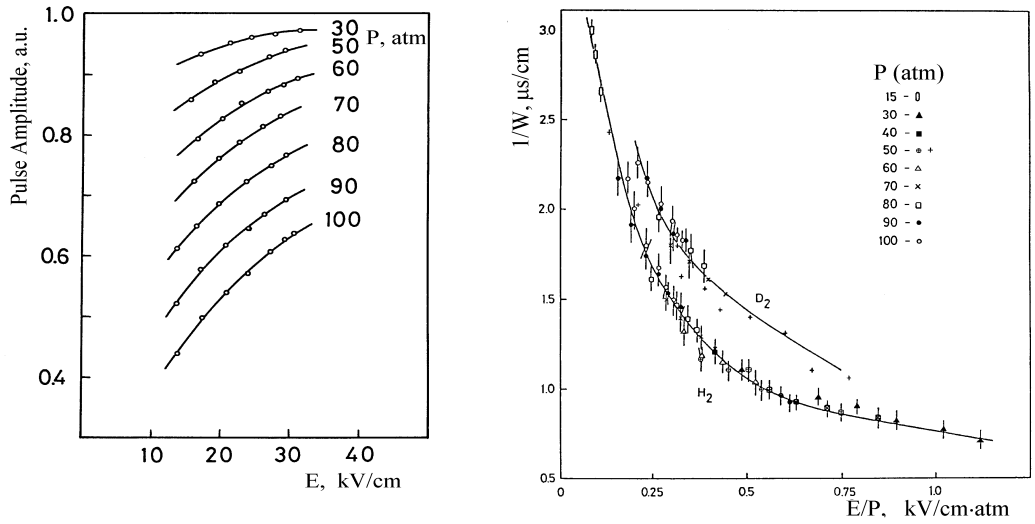

Figure 8: Recombination and Drift velocity from Ref. [4]. The MuSun conditions correspond to P=50 atm, E=10 kV/cm and E/P= 0.2 kV/cm-atm.

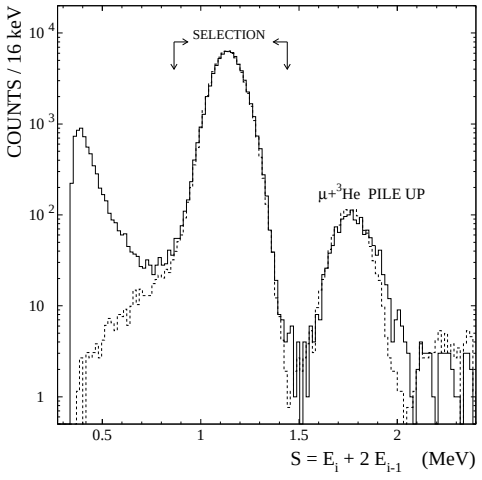

Figure 9: Placeholder, needs simulation of MuSun geometry. Properties of Muon Stops in TPC

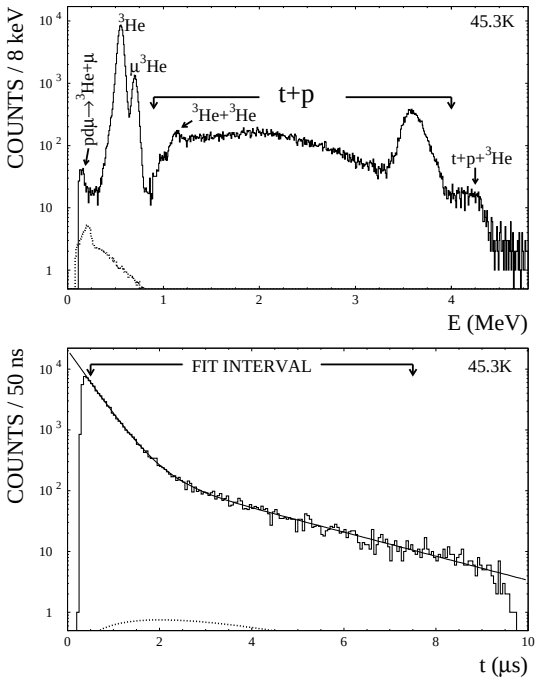

Figure 10: Charged particle spectra after muon stop from Ref. [4]. The conditions were T=45.3 K, ϕ=0.0524 and nitrogen impurity level $c_N \approx 41$ ppb.

7 Statistics and Systematics

7.1 Statistics and Rates

case		N_- (10^{10})	N_+ (10^{10})	weeks beam time
1	λ_μ^-, λ_μ^+ measured in MuSun	1.8	1.8	20
2	λ_μ^- from MuSun, λ_μ^+ with 1 ppm from MuLan	1.3	-	7

Table 4: Statistics estimate for primary data taking for two cases considered. N_- (N_+) are the statistics of fully reconstructed μ^- (μ^+) decay events $\mu \to ev\bar{\nu}$ after all selection cuts have been applied.

The MuSun experiment will measure Λ_d to 1%. Thus $\delta\lambda = \lambda_\mu^- - \lambda_\mu^+$ has to be measured to a precision of 4 s^{-1} or 8.8 ppm of λ_μ^+. Tab.4 presents the required statistics for two cases. Case 1 is the more conservative approach, i.e. λ_μ^+ is also measured in the same apparatus with the required statistics to cancel most of the instrumental systematics. In case 2, only λ_μ^- is measured, the positive muon lifetime is taken with the expected precision of the final MuLan result. The last column indicates the total measuring time for primary data taking. Based on MuCap experience about 8 weeks total will be needed for systematics studies, calibrations, background measurements, set-up and pumping time for this complex high precision experiment. The measurement schedule will be detailed in the beam-time requests at a later time. In total the experiment will require two to three 12 week data taking runs, once the full set-up is commissioned.

rate	(kHz)	relative efficiency
μSC entrance scintillator	27	
& full pile-up protected $\mu SC \times \mu PC$	22	ϵ_1=0.8
& stop in TPC fiducial volume	12	ϵ_2=0.54
& fully reconstructed electron	5.4	ϵ_3=0.37

Table 5: Event rates and efficiencies ϵ for different selection levels, where ϵ is the ratio between rate after/before selection. BRENDAN, why is ϵ_3 so low?

The translation of statistics into measuring time follows the rates achieved in MuCap. Typically 2×10^9 events were collected in one week. Table 5 compiles the factors contributing to the final rates. We are optimizing the new set-up to improve ϵ_2, because of the higher gas density. Moreover, the experiment will benefit from the increase in proton current at PSI anticipated during the next years.

The MuSun experiment will also derive essential information from the time distributions of capture and fusion products. Their statistics is estimated based on a total number of stopped muons N in the TPC calculated as

$$N = \frac{N_-}{\epsilon_3} \tag{16}$$

which, for N_-=1.3$\times$ 10^{10}, amounts to 3.5$\times$ 10^{10}. As rough estimate of the expected time distribution and statistics are given in fig.11 and table 6.

process	distribution	yield/μ	efficiency estimate	total observed events
$\mu \to e\nu\bar{\nu}$	el(t)	0.9992	0.37	1.3$\times$ 10^{10}
$dd\mu \to {}^3He + n + \mu$	fus(t)	0.0305	1.00	1.1$\times$ 10^9
$\mu + d \to n + n + \nu$	capN(t)	0.0015	0.02	1.1$\times$ 10^6
$\mu + {}^3He \to t + \nu$	capT(t)	1.2$\times$ 10^{-5}	1.00	4.3$\times$ 10^5
$\mu + N \to C^* + \nu$				3.5$\times$ 10^5

Table 6: Total number of events for different processes based on N=3.5$\times$ 10^{10} and estimated detection efficiencies (column 3). The impurity capture events are based on typical MuCap conditions of 10^{-5} observed captures/muon. The impurity level should improve at low T=30 K.

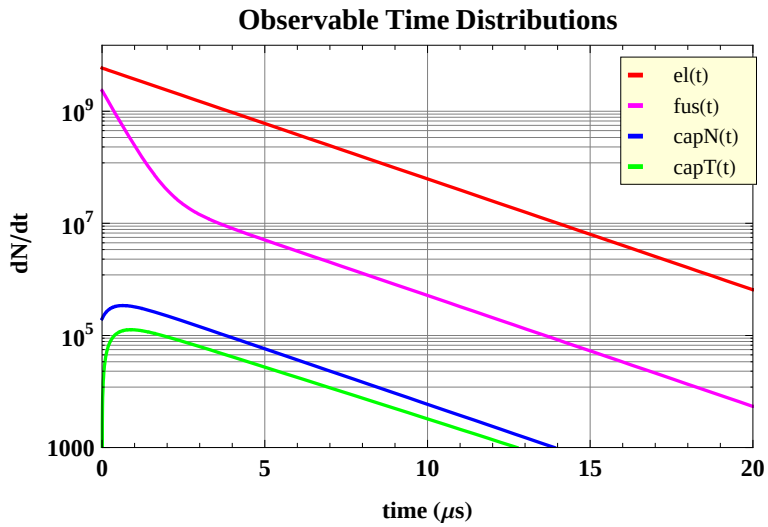

Figure 11: Observable time distributions for total good muon statistics N=3.5× 10^{10}.

7.2 Systematics

Table 7 separates the systematic issues for the MuSun experiment into three categories. For each categories the achieved precision of the first MuCap result is given in column 2, the anticipated precision of the final MuCap results (based on data already taken and ongoing analyses) is estimated in column 3 and the projected uncertainty of the MuSun experiment are presented in the last column.

1. For systematics common to both experiments, only cases which differ between MuSun and MuCap are discussed below.
2. Systematics unique to MuCap is not discussed any further.
3. Systematics specific for MuSun will be detailed below.

7.2.1 Clean Muon Stop

Needs careful discussion of the charged recoils, the much poorer pad spatial resolution, the large potential muon energy deposit etc. This is coupled with pad TPC optimization.

7.2.2 Chemical Gas purity

Purity needs to be discussed carefully according to table 8. Using delayed time window in fig.10 reduces He background 10 fold. Requiring no electron by 1.4. Perhaps this factor 14 is sufficient for 1 ppb sensitivity. Additional tagging (X-ray, capture FADC signature, capture neutron) needs to be worked out. ^{3}He tail can be measured precisely with survived muon method.

7.2.3 Isotopic Gas purity

Should be straight forward.

7.2.4 Hyperfine transition + μ^3He capture

Already done above

7.2.5 Fusion Processes

Influence on muon signals discussed above. Discuss precision of time distributions, i.e. extra information here.

Topic	MuCap 2007	MuCap Final	MuSun
Statistics	12.59	5.63	
Similar for MuCap and MuSun			
chemical impurities	5.25	2	XX *
overall consistency	5	1	1
unseen scatter	3	1	1
mu track def	2	1	XX *
entrance counter ineff	2.5	2	1
bound state corr	0	0	0
kicker issues	0	1	1
λ_μ^+	4.35	0.68	0.68
MuCap only			
md diff	1.58	1.58	
mp diff	0.46	0.46	
λ_{OF} corr	5	0.2	
λ_{OP} corr	2		
MuSun only			
md diff			XX *
^{1}H contamination			XX *
fusion processes			XX *
hyperfine transition			XX *
μ^3He capture			XX *
total stat error	13.32	5.67	
total sys error	11.41	4.72	

Table 7: Comparison of the systematic uncertainties (in s^{-1}). Specific MuSun issues, different from the MuCap experimental conditions, are marked by * and evaluated in this section.

Nucleus	E (eV)	$\lambda_p Z$ ($10^{10} s^{-1}$)	Ref	$\lambda_d Z$ ($10^{10} s^{-1}$)	Ref
N	0.04	3.4 ± 0.7		14.5 ± 0.2	
O	0.04	8.5 ± 0.2		6.3 ± 0.5	

Table 8: Muon transfer rates from μp and μd atoms to N and O, respectively. Transfer rates given for thermal energies, as thermalization is much faster than transfer at MuSun experimental conditions.

8 Measuring Program

8.1 Stage 1

The experiment will proceed in two stages. First we will prepare a prototype of the new pad TPC. The pad plane layout and Frisch grid will be identical to the final TPC, but the chamber will operate at room temperature at density ϕ=1% (MuCap conditions). The detector will be reconfiguration of the second TPC, which the collaboration prepared for the MuCap experiment [2]. We request 10 weeks of beam time for commissioning and physics running with this new chambers. Essential technical goals of this stage include

- Demonstrate excellent resolution and muon identification with new TPC operated as ionization chamber.
- Identification and separation of fusion recoils.
- Full analog readout of whole TPC in untriggered mode.

The physics goals are as follows

- Initial capture rate measurement.

[2]The first MuCap TPC, used in our ultrapure protium measurements, will be left untouched

- Observation of residual polarization of muons in μd quartet state.
- Measurement of tranfer rate from deuterium to nitrogen.
- Attempt to monitor impurities by detection of capture events in the presence of fusion background.

8.2 Stage 2

By fall of 2009 we should be ready for a first run with the high density cryo TPC.

9 Organization

9.1 Responsibilities

People and hardware

9.2 Budget Draft

9.3 Time Line

9.4 Request to PSI

10 First Beam Request

11 References

References

[1] J. Adam, E. Truhlik, S. Ciechanowicz, and K. M. Schmitt. Muon capture in deuterium and the meson exchange current effect. *Nucl. Phys.*, A507:675–697, 1990.

[2] S. Ando, T. S. Park, K. Kubodera, and F. Myhrer. The mu- d capture rate in effective field theory. *Phys. Lett.*, B533:25–36, 2002.

[3] V. A. Andreev et al. Measurement of the rate of muon capture in hydrogen gas and determination of the proton's pseudoscalar coupling g_p. *Phys. Rev. Lett.*, 99:032002, 2007.

[4] D.V. Balin et al. *PNPI Preprint*, 2729, 2007.

[5] G. Bardin et al. A measurement of the rate of muon capture in liquid deuterium by the lifetime technique. *Nucl. Phys.*, 1986.

[6] A. Bertin, A. Vitale, A. Placci, and E. Zavattini. Muon capture in gaseous deuterium. *Phys. Rev.*, D8:3774–3793, 1973.

[7] W. H. Breunlich, P. Kammel, J. S. Cohen, and M. Leon. Muon-catalyzed fusion. *Ann. Rev. Nucl. Part. Sci.*, 39:311–356, 1989.

[8] K. I. T. Brown, M. N. Butler, and D. B. Guenther. Constraints on proton-proton fusion from helioseismology. 2002.

[9] Malcolm Butler, Jiunn-Wei Chen, and Petr Vogel. Constraints on two-body axial currents from reactor antineutrino deuteron breakup reactions. *Phys. Lett.*, B549:26–31, 2002.

[10] M. Cargnelli et al. In *Proceedings of the XXIII Yamada Conf. on Nuclear Weak Processes and Nuclear Structure, Osaka*.

[11] Jiunn-Wei Chen, Karsten M. Heeger, and R. G. Hamish Robertson. Constraining the leading weak axial two-body current by sno and super-k. *Phys. Rev.*, C67:025801, 2003.

[12] Jiunn-Wei Chen, Takashi Inoue, Xiang-dong Ji, and Ying-chuan Li. Fixing two-nucleon weak-axial coupling $l_{1,A}$ from mu-d capture. *Phys. Rev.*, C72:061001, 2005.

[13] Andrzej Czarnecki, William J. Marciano, and Alberto Sirlin. Electroweak radiative corrections to muon capture. *Phys. Rev. Lett.*, 99:032003, 2007.

[14] M. Doi, T. Sato, H. Ohtsubo, and M. Morita. Effect of meson exchange current on deuteron - muon capture. *Nucl. Phys.*, A511:507, 1990.

[15] D. E. Gonzalez Trotter et al. Neutron-deuteron breakup experiment at e(n) = 13-mev: Determination of the (1)s(0) neutron-neutron scattering length ann. *Phys. Rev.*, C73:034001, 2006.

[16] P. Kammel et al. First observation of muonic hyperfine effects in pure deuterium. *Phys. Rev.*, A28:2611–2622, 1983.

[17] R. Machleidt and I. Slaus. The nucleon nucleon interaction. *J. Phys.*, G27:R69, 2001.

[18] L. E. Marcucci et al. Weak proton capture on 3he. *Phys. Rev.*, C63:015801, 2001.

[19] L. E. Marcucci, R. Schiavilla, S. Rosati, A. Kievsky, and M. Viviani. Theoretical study of the he-3(mu-,nu/mu)h-3 capture. *Phys. Rev.*, C66:054003, 2002.

[20] R. Schiavilla et al. Weak capture of protons by protons. *Phys. Rev.*, C58:1263, 1998.

[21] N. Tatara, Y. Kohyama, and K. Kubodera. Weak interaction processes on deuterium: Muon capture and neutrino reactions. *Phys. Rev.*, C42:1694–1717, 1990.

[22] I.-T. Wang et al. *Phys. Rev.*, 1965.

12 Appendix

12.1 Additional Physics Opportunities

Few-body and Astrophysics

Form Factors

Technology